International Journal of Heat and Mass Transfer 52 (2009) 45–55

Contents lists available at ScienceDirect

International Journal of Heat and Mass Transfer

journal homepage: www.elsevier.com/locate/ijhmt

Conjugated heat transfer in double-pass laminar counterflow concentric-tube heat exchangers with sinusoidal wall fluxes

Chii-Dong Ho *, Jr-Wei Tu, Chih-Ming Yang

Energy and Opto-Electronic Materials Research Center, Department of Chemical and Materials Engineering, Tamkang University, Tamsui, Taipei 251, Taiwan

ARTICLE INFO

Article history:
Received 4 April 2008
Received in revised form 31 May 2008
Available online 30 July 2008

Keywords:
Sinusoidal heat fluxes
Conjugated Graetz problems
Double-pass operation
Concentric circular heat exchanger

ABSTRACT

An analytical method is proposed to predict the temperature distribution and local Nusselt number for laminar flow in a double-pass countercurrent heat exchanger with sinusoidal heat flux distribution. A design of inserting in parallel an impermeable barrier to divide an open conduit into two subchannels for conducting double-pass operations, resulting in substantially improved the heat transfer rate, has been evaluated theoretically in the fully developed region. Comparison with the theoretical results shows that the heat-transfer efficiency improvement for double-pass concentric circular heat exchangers is generally higher than those in the single-pass operations without an impermeable barrier inserted. The influences of the impermeable-barrier location on the heat-transfer efficiency improvement and power consumption increment, as indicated from theoretical predictions, can be used to determine the economical feasibility in operating double-pass devices.

1. Introduction

The studies on the heat-transfer phenomena of fluid flow in a bounded conduit are essential to the improved design of heat transfer equipment. The theoretical model coupled with the analytical solution or numerical results are useful to obtain the convective heat-transfer coefficients estimation and temperature distribution under different physical conditions. The well-known Graetz problems [1–3] study the heat transfer system with laminar flow of the negligible axial conduction in cylindrical or parallel-plate geometries. For low Prandtl number fluids, such as liquid metal, the effects of axial conduction cannot be ignored in analysis of heat-transfer phenomenon and such problems are so-called extended Graetz problems [4–6]. Moreover, the laminar convective heat transfer of multi-stream or multiphase systems are called conjugated Graetz problems [7–9].

Much effort has been devoted to investigate the different kinds of boundary conditions which can be prescribed at the conduit wall. Most of the interest on the heat transfer in engineering applications is the two cases of the uniform wall temperature (Dirichlet problem) [10,11] and uniform heat flux (Neumann problem) [12–14]. However, the convective heat-transfer problems with non-uniform heating are also investigated by many researchers, such as asymmetric heating [15,16], periodic heating [17,18] and circumferentially heating [19,20]. The condition of periodic heating is usually occurs in pre-heating systems and experimental setups with employing the equally spacing heating strips. The simplest model of period heating is the sinusoidal wall heat flux [21,22] or sinusoidal temperature distribution [23]. The well-known case of sinusoidal wall heat flux distribution on the wall is in the designing of the cooling tubes in nuclear reactors.

In the present study, an impermeable barrier was inserted to divide an open conduit into two subchannels for conducting double-pass operations to improve the heat transfer rate of the tube heat exchangers with sinusoidal wall fluxes. The purposes of this study are (1) to develop a theoretical mathematical model of double-pass laminar counterflow concentric-tube heat exchangers with sinusoidal wall fluxes; (2) to solve analytically the wall temperature distribution in flow direction; (3) to discuss the effects of Graetz number and impermeable-barrier location on the Nusselt number and heat-transfer efficiency improvement.

2. Temperature distributions

A double-pass concentric-tube heat exchanger was made by inserting an impermeable barrier into a circular tube of inside diameter $2R$ and length L, as shown in Fig. 1. The thickness of the inner (subchannel a) and annular tube (subchannel b) are $2\kappa R$ and $2(1-\kappa)R$, respectively. Comparing to the radius of circular tube R, the thickness of the impermeable barrier δ is negligible ($\delta \ll R$). Two flow patterns, say flow pattern A and flow pattern B, are proposed in this study. The flow pattern A is that the fluid with volumetric flow rate V and temperature T_1 firstly feeds into subchannel a and then flows reversely into the subchannel b with

* Corresponding author. Fax: +886 2 26209887.
E-mail address: cdho@mail.tku.edu.tw (C.-D. Ho).

0017-9310/$ - see front matter © 2008 Elsevier Ltd. All rights reserved.
doi:10.1016/j.ijheatmasstransfer.2008.05.036

Nomenclature

a_n	coefficient in Eq. (40)
b_n	coefficient in Eq. (41)
B	constant, defined in Eq. (13)
D_e	equivalent diameter of the conduit, m
f	friction factor
Gz	Graetz Number, $4V/\alpha\pi L$
h	heat-transfer coefficient kW/m^2 K
I_h	heat transfer improvement based on single-pass devices, defined by Eq. (66)
I_p	power consumption increment, defined by Eq. (68)
k	heat conductivity coefficient of the wall, kW/m K
L	conduit length, m
ℓw_f	friction loss in conduit, N m/kg
$\mathrm{Nu}(\xi)$	local Nusselt number, defined by Eq. (59)
$\overline{\mathrm{Nu}}$	average Nusselt number, defined by Eq. (64)
P	power consumption, N m/s
q''	heat flux on the wall, J/m^2 s
R	radius of outer tube, m
r	radial coordinate, m
R_1	radius of inner tube, m
Re	Reynolds number
T	temperature, K
u	velocity distribution of fluid, m/s
$\bar{u}$	average velocity of fluid, m/s
V	input volume flow rate of conduit, m^3/s
W_1	constant, defined in Eq. (7)
W_2	constant, defined in Eq. (8)
z	longitudinal coordinate, m

Greek symbols

α	thermal diffusivity of fluid, m^2/s
β	constant
δ	impermeable barrier thickness, m
ϕ	dimensionless temperature, $k(T-T_i)/q''_0R$
γ_{1a}, γ_{2a}	integration constants in Eq. (53)
γ_{1b}, γ_{2b}	integration constants in Eq. (54)
η	radial coordinate, r/R
κ	impermeable-barrier location, defined in Eq. (13)
λ	constant
θ_{0a}	constant in Eq. (14)
θ_{0b}	constant in Eq. (15)
θ_{1a}, θ_{2a}, θ_{3a}	functions of η, defined in Eq. (14)
θ_{1b}, θ_{2b}, θ_{3b}	functions of η, defined in Eq. (15)
ξ	longitudinal coordinate, $z/(LGz)$

Subscripts

a	subchannel a
b	subchannel b
F	at the outlet
i	at the inlet
0	in a single-pass device without recycle
w	at the wall surface

the aid of a convectional pump at the end of the conduit as shown in Fig. 1(a). In other hand, the flow pattern B is that the fluid firstly feeds into subchannel b and exits from the subchannel a as shown in Fig. 1(b). In both flow patterns, the fluid is heated by the outer wall with sinusoidal heat fluxes, $q''_w(z) = q''_0[1+\sin(\beta z)]$.

The following assumptions are made to simplify the theoretical analysis: constant physical properties of fluid; fully-developed laminar flow in the entire length in the inner and annular subchannels; neglecting the entrance length and the end effects; ignoring the longitudinal heat conduction and the thermal resistance of the impermeable barrier.

The energy balance equations of a double-pass heat exchanger with sinusoidal heat fluxes were formulated as

$$\frac{u_a(\eta)R^2}{GzL\alpha}\frac{\partial\phi_a(\eta,\xi)}{\partial\xi} = \frac{1}{\eta}\frac{\partial}{\partial\eta}\left(\eta\frac{\partial\phi_a(\eta,\xi)}{\partial\eta}\right) \tag{1}$$

$$\frac{u_b(\eta)R^2}{GzL\alpha}\frac{\partial\phi_b(\eta,\xi)}{\partial\xi} = \frac{1}{\eta}\frac{\partial}{\partial\eta}\left(\eta\frac{\partial\phi_b(\eta,\xi)}{\partial\eta}\right) \tag{2}$$

where u_a and u_b are the velocity distributions in subchannels a and b, respectively, which are derived in Appendix A, and they are

$$u_a(\eta) = \frac{2V}{\pi(\kappa R)^2}\left(1-\left(\frac{\eta}{\kappa}\right)^2\right) \quad 0\leqslant\eta_a\leqslant\kappa \tag{3}$$

$$u_b(\eta) = -\frac{2V}{[\pi R^2-\pi(\kappa R)^2]W_1}\left[1-(\eta)^2+W_2\ln\eta\right] \quad \kappa\leqslant\eta_b\leqslant 1 \tag{4}$$

in flow pattern A and

$$u_a(\eta) = \frac{-2V}{\pi(\kappa R)^2}\left(1-\left(\frac{\eta}{\kappa}\right)^2\right) \quad 0\leqslant\eta_a\leqslant\kappa \tag{5}$$

$$u_b(\eta) = \frac{2V}{\left[\pi R^2-\pi(\kappa R)^2\right]W_1}[1-(\eta)^2+W_2\ln\eta] \quad \kappa\leqslant\eta_b\leqslant 1 \tag{6}$$

in flow pattern B, respectively, where W_1 and W_2 are

$$W_1 = \left[\frac{1-\kappa^4}{1-\kappa^2}-\frac{1-\kappa^2}{\ln\frac{1}{\kappa}}\right] \tag{7}$$

and

$$W_2 = \left(\frac{1-\kappa^2}{\ln 1/\kappa}\right) \tag{8}$$

The corresponding boundary conditions are

$$\frac{\partial\phi_a(0,\xi)}{\partial\eta} = 0 \tag{9}$$

$$\frac{\partial\phi_b(1,\xi)}{\partial\eta} = 1+\sin(B\xi) \tag{10}$$

$$\frac{\partial\phi_a(\kappa,\xi)}{\partial\eta} = \frac{\partial\phi_b(\kappa,\xi)}{\partial\eta} \tag{11}$$

$$\phi_a(\kappa,\xi) = \phi_b(\kappa,\xi) \tag{12}$$

The dimensionless groups in Eqs. (1)–(12) are

$$\eta = \frac{r}{R}, \quad \xi = \frac{z}{GzL}, \quad \phi_a = \frac{k(T_a-T_i)}{q''_0R}, \quad \phi_b = \frac{k(T_b-T_i)}{q''_0R},$$
$$Gz = \frac{4V}{\alpha\pi L}, \quad \kappa = \frac{R_1}{R}, \quad B = \beta GzL \tag{13}$$

The dimensionless temperature distribution of the laminar double-pass counterflow concentric-tube heat exchangers with sinusoidal wall fluxes can be expressed as follows: [14,22]

$$\phi_a(\eta,\xi) = \theta_{0a}\xi+\theta_{1a}(\eta)+\theta_{2a}(\eta)\sin(B\xi) + \theta_{3a}(\eta)\cos(B\xi) \tag{14}$$

$$\phi_b(\eta,\xi) = \theta_{0b}\left(\frac{1}{Gz}-\xi\right)+\theta_{1b}(\eta)+\theta_{2b}(\eta)\sin(B\xi) + \theta_{3b}(\eta)\cos(B\xi) \tag{15}$$

in which the θ_{0a} and θ_{0b} are the undetermined constants, and the θ_{1a}, θ_{2a}, θ_{3a}, θ_{1b}, θ_{2b} and θ_{3b} are the functions of η to be deter-

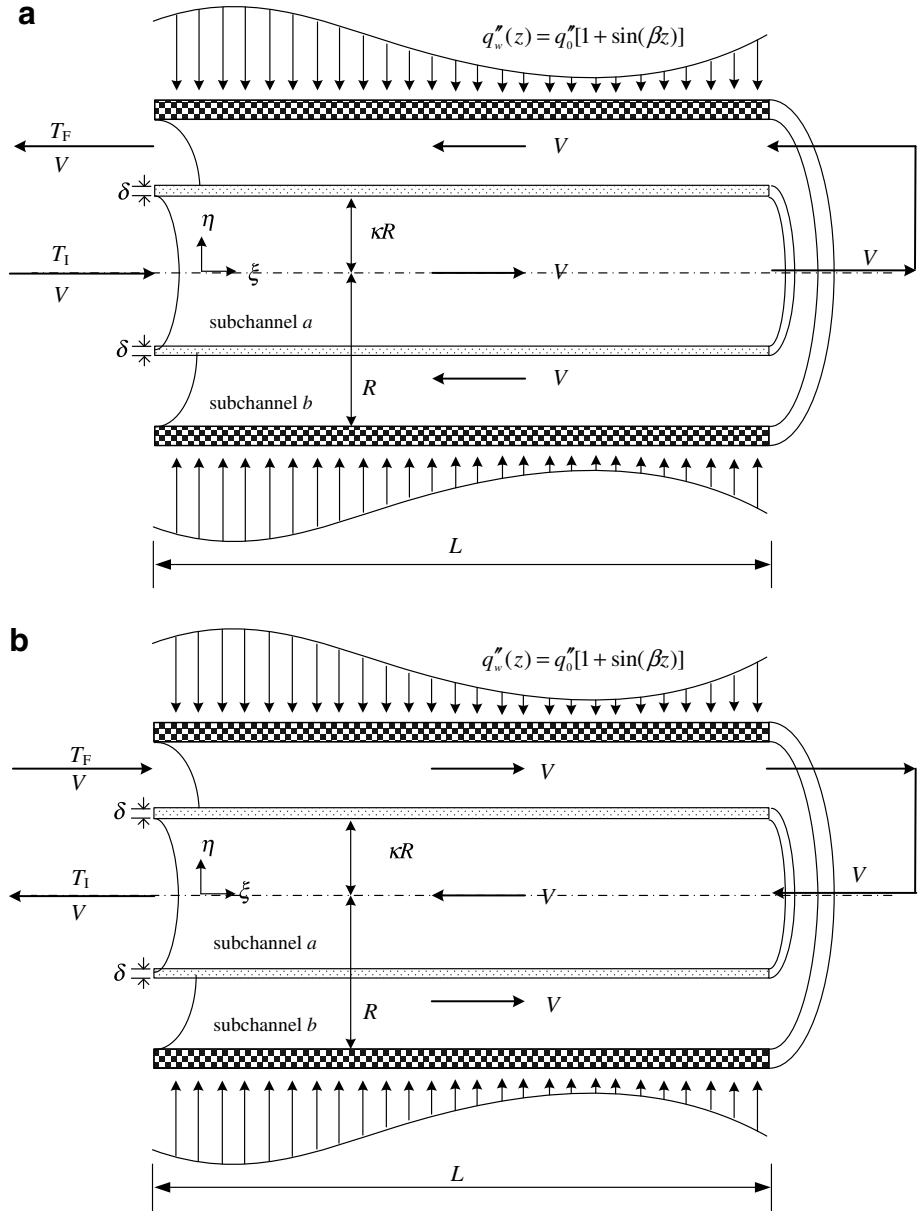

Fig. 1. Double-pass concentric-tube heat exchangers with sinusoidal wall fluxes.

mined. Substituting Eqs. (14) and (15) into the governing equations, Eqs. (1) and (2), and the boundary conditions, Eqs. (9)–(12), yields

$$\frac{\mathrm{d}}{\mathrm{d}\eta}\left(\eta\frac{\mathrm{d}\theta_{1a}(\eta)}{\mathrm{d}\eta}\right)-\frac{u_a(\eta)R^2\eta}{GzL\alpha}\theta_{0a}+\left[\frac{\mathrm{d}}{\mathrm{d}\eta}\left(\eta\frac{\mathrm{d}\theta_{2a}(\eta)}{\mathrm{d}\eta}\right)+\frac{u_a(\eta)BR^2\eta}{GzL\alpha}\theta_{3a}(\eta)\right]\sin(B\xi)+\left[\frac{\mathrm{d}}{\mathrm{d}\eta}\left(\eta\frac{\mathrm{d}}{\theta_{3a}(\eta)}\mathrm{d}\eta\right)-\frac{u_a(\eta)BR^2\eta}{GzL\alpha}\theta_{2a}(\eta)\right]\cos(B\xi)=0 \quad (16)$$

$$\frac{\mathrm{d}}{\mathrm{d}\eta}\left(\eta\frac{\mathrm{d}\theta_{1b}(\eta)}{\mathrm{d}\eta}\right)+\frac{u_b(\eta)R^2\eta}{GzL\alpha}\theta_{0b}+\left[\frac{\mathrm{d}}{\mathrm{d}\eta}\left(\eta\frac{\mathrm{d}\theta_{2b}(\eta)}{\mathrm{d}\eta}\right)+\frac{u_b(\eta)BR^2\eta}{GzL\alpha}\theta_{3b}(\eta)\right]\sin(B\xi)+\left[\frac{\mathrm{d}}{\mathrm{d}\eta}\left(\eta\frac{\mathrm{d}\theta_{3b}(\eta)}{\mathrm{d}\eta}\right)-\frac{u_b(\eta)BR^2\eta}{GzL\alpha}\theta_{2b}(\eta)\right]\cos(B\xi)=0 \quad (17)$$

$$\frac{\mathrm{d}\theta_{1a}(0)}{\mathrm{d}\eta}+\frac{\mathrm{d}\theta_{2a}(0)}{\mathrm{d}\eta}\sin(B\xi)+\frac{\mathrm{d}\theta_{3a}(0)}{\mathrm{d}\eta}\cos(B\xi)=0 \quad (18)$$

$$\left(\frac{\mathrm{d}\theta_{1\,b}(1)}{\mathrm{d}\eta}-1\right)+\left(\frac{\mathrm{d}\theta_{2\,b}(1)}{\mathrm{d}\eta}-1\right)\sin(B\xi)+\left[\frac{\mathrm{d}\theta_{3b}(1)}{\mathrm{d}\eta}\right]\cos(B\xi)=0 \quad (19)$$

$$\left(\frac{\mathrm{d}\theta_{1a}(\kappa)}{\mathrm{d}\eta}-\frac{\mathrm{d}\theta_{1b}(\kappa)}{\mathrm{d}\eta}\right)+\left(\frac{\mathrm{d}\theta_{2a}(\kappa)}{\mathrm{d}\eta}-\frac{\mathrm{d}\theta_{2b}(\kappa)}{\mathrm{d}\eta}\right)\sin(B\xi)+\left(\frac{\mathrm{d}\theta_{3a}(\kappa)}{\mathrm{d}\eta}-\frac{\mathrm{d}\theta_{3b}(\kappa)}{\mathrm{d}\eta}\right)\cos(B\xi)=0 \quad (20)$$

$$\theta_{0a}\xi+\theta_{1a}(\kappa)+\theta_{2a}(\kappa)\sin(B\xi)+\theta_{3a}(\kappa)\cos(B\xi)=\theta_{0b}\left(\frac{1}{Gz}-\xi\right)+\theta_{1b}(\kappa)+\theta_{2b}(\kappa)\sin(B\xi)+\theta_{3b}(\kappa)\cos(B\xi) \quad (21)$$

2.1. Solving $\theta_{2a}(\eta)$, $\theta_{3a}(\eta)$, $\theta_{2b}(\eta)$ and $\theta_{3b}(\eta)$ by Frobenius method

Multiplying Eqs. (16)–(21) by $\sin(B\xi)$ and integrating with respect to ξ in the interval $[0,2\pi/B]$, one can obtain

$$\frac{d}{d\eta}\left(\eta\frac{d\theta_{2a}(\eta)}{d\eta}\right)+\frac{u_a(\eta)BR^2\eta}{GzL\alpha}\theta_{3a}(\eta)=0 \tag{22}$$

$$\frac{d}{d\eta}\left(\eta\frac{d\theta_{2b}(\eta)}{d\eta}\right)+\frac{u_b(\eta)BR^2\eta}{GzL\alpha}\theta_{3b}(\eta)=0 \tag{23}$$

$$\frac{d\theta_{2a}(0)}{d\eta}=0 \tag{24}$$

$$\frac{d\theta_{2b}(1)}{d\eta}=1 \tag{25}$$

$$\frac{d\theta_{2a}(\kappa)}{d\eta}=\frac{d\theta_{2b}(\kappa)}{d\eta} \tag{26}$$

$$\theta_{2a}(\kappa)=\theta_{2b}(\kappa) \tag{27}$$

Similarly, multiplying Eqs. (16)–(21) by $\cos(B\xi)$ and integrating with respect to ξ in the interval $[0,2\pi/B]$, one can obtain

$$\frac{d}{d\eta}\left(\eta\frac{d\theta_{3a}(\eta)}{d\eta}\right)-\frac{u_a(\eta)BR^2\eta}{GzL\alpha}\theta_{2a}(\eta)=0 \tag{28}$$

$$\frac{d}{d\eta}\left(\eta\frac{d\theta_{3b}(\eta)}{d\eta}\right)-\frac{u_b(\eta)BR^2\eta}{GzL\alpha}\theta_{2b}(\eta)=0 \tag{29}$$

$$\frac{d\theta_{3a}(0)}{d\eta}=0 \tag{30}$$

$$\frac{d\theta_{3b}(1)}{d\eta}=0 \tag{31}$$

$$\frac{d\theta_{3a}(\kappa)}{d\eta}=\frac{d\theta_{3b}(\kappa)}{d\eta} \tag{32}$$

$$\theta_{3a}(\kappa)=\theta_{3b}(\kappa) \tag{33}$$

According to the mathematical treatment in the previous work [22], the complex functions $\psi_a(\eta)=\theta_{2a}(\eta)+\theta_{3a}(\eta)i$ and $\psi_b(\eta)=\theta_{2b}(\eta)+\theta_{3b}(\eta)i$ were introduced to combine Eqs. (22)–(27) and Eqs. (28)–(33) into a unique one-dimensional boundary value problem as follows:

$$\frac{d}{d\eta}\left(\eta\frac{\partial\psi_a(\eta)}{\partial\eta}\right)-\frac{u_a(\eta)BR^2\eta}{GzL\alpha}\psi_a(\eta)i=0 \tag{34}$$

$$\frac{d}{d\eta}\left(\eta\frac{\partial\psi_b(\eta)}{\partial\eta}\right)-\frac{u_b(\eta)BR^2\eta}{GzL\alpha}\psi_b(\eta)i=0 \tag{35}$$

$$\frac{d\psi_a(0)}{d\eta}=0 \tag{36}$$

$$\frac{d\psi_b(1)}{d\eta}=1 \tag{37}$$

$$\frac{d\psi_a(\kappa)}{d\eta}=\frac{d\psi_b(\kappa)}{d\eta} \tag{38}$$

$$\psi_a(\kappa)=\psi_b(\kappa) \tag{39}$$

By applying the Frobenius method, the $\psi_a(\eta)$ and $\psi_b(\eta)$ can be expressed as

$$\psi_a(\eta)=\sum_{n=0}^{\infty}a_n\eta^{n+\lambda_a},\quad n\geqslant 0 \tag{40}$$

$$\psi_b(\eta)=\sum_{n=0}^{\infty}b_n\eta^{n+\lambda_b},\quad n\geqslant 0 \tag{41}$$

As provided in Appendix B, one can find the constants of λ_a and λ_b are zero. For the flow pattern A, the coefficients a_n and b_n are determined by following recursive relations

$$a_0,\quad a_{2n}=\frac{Bi}{8\kappa^2}\frac{1}{n^2}\left(a_{2n-2}-\frac{1}{\kappa^2}a_{2n-4}\right),\quad n\geqslant 1 \tag{42}$$

and

$$b_0,\quad b_1=0,\quad b_n=\frac{-Bi}{2W_1(1-\kappa^2)}\frac{1}{n^2}\left[\left(1-\frac{3}{2}W_2\right)b_{n-2}+2W_2b_{n-3}-\left(1+\frac{1}{2}W_2\right)b_{n-4}\right],\quad n\geqslant 2, \tag{43}$$

respectively. Moreover, for the flow pattern B, the recursive relations of the coefficients a_n and b_n are

$$a_0,\quad a_{2n}=\frac{-Bi}{8\kappa^2}\frac{1}{n^2}\left(a_{2n-2}-\frac{1}{\kappa^2}a_{2n-4}\right),\quad n\geqslant 1 \tag{44}$$

and

$$b_0,\quad b_1=0,\quad b_n=\frac{Bi}{2W_1(1-\kappa^2)}\frac{1}{n^2}\left[\left(1-\frac{3}{2}W_2\right)b_{n-2}+2W_2b_{n-3}-\left(1+\frac{1}{2}W_2\right)b_{n-4}\right],\quad n\geqslant 2 \tag{45}$$

The undetermined coefficients a_0 and b_0 in Eqs. (42)–(45) can be solved by the boundary conditions. Hence, the expressions of $\theta_{2a}(\eta)$, $\theta_{3a}(\eta)$, $\theta_{2b}(\eta)$ and $\theta_{3b}(\eta)$ were obtained by substituting Eqs. (42) and (43) (flow pattern A) and Eqs. (44) and (45) (flow pattern B) into Eqs. (40) and (41), respectively.

2.2. Solving θ_{0a}, $\theta_{1a}(\eta)$, θ_{0b} and $\theta_{1b}(\eta)$

The functions of $\theta_{1a}(\eta)$ and $\theta_{1b}(\eta)$ and constants θ_{0a} and θ_{0b} can be solved by following procedure. Firstly, by integrating Eqs. (16)–(21) with respect to ξ in the interval $[0,2\pi/B]$, one can obtain

$$\frac{d}{d\eta}\left(\eta\frac{d\theta_{1a}(\eta)}{d\eta}\right)-\frac{u_a(\eta)R^2\eta}{GzL\alpha}\theta_{0a}=0 \tag{46}$$

$$\frac{d}{d\eta}\left(\eta\frac{d\theta_{1b}(\eta)}{d\eta}\right)+\frac{u_b(\eta)R^2\eta}{GzL\alpha}\theta_{0b}=0 \tag{47}$$

$$\frac{d\theta_{1a}(0)}{d\eta}=0 \tag{48}$$

$$\frac{d\theta_{1b}(1)}{d\eta}=1 \tag{49}$$

$$\frac{d\theta_{1a}(\kappa)}{d\eta}=\frac{d\theta_{1b}(\kappa)}{d\eta} \tag{50}$$

$$\theta_{0a}=-\theta_{0b} \tag{51}$$

$$\theta_{1a}(\kappa)=\frac{\theta_{0b}}{Gz}+\theta_{1\ b}(\kappa) \tag{52}$$

Then, integrating Eqs. (46) and (47) twice with respect to η for $\theta_{1a}(\eta)$ and $\theta_{1b}(\eta)$ yields

$$\theta_{1a}=\frac{\theta_{0\ a}}{2\kappa^2}\left[\frac{1}{4}\eta^2-\frac{\eta^4}{16\kappa^2}+\gamma_{1a}\ln\eta+\gamma_{2\ a}\right] \tag{53}$$

and

$$\theta_{1b}=\frac{\theta_{0b}}{2W_1(1-\kappa^2)}\left[\frac{1}{4}\eta^2-\frac{1}{16}\eta^4+\frac{W_2}{4}\eta^2[\ln\eta-1]+\gamma_{1b}\ln\eta+\gamma_{2b}\right] \tag{54}$$

respectively, where γ_{1a}, γ_{2a}, γ_{1b} and γ_{2b} are the integrating constants. The two undetermined constants θ_{0a} and θ_{0b}, and the four integrating constants γ_{1a}, γ_{2a}, γ_{1b} and γ_{2b} were calculated by the boundary conditions, Eqs. (48)–(52), and the overall energy balance

$$\rho C_p V(T_F-T_i)=\int_0^L q''(z)2\pi R dz \tag{55}$$

or rewritten as

$$\phi_F=\int_0^{\frac{1}{Gz}}8[1+\sin(B\xi)]d\xi=8\left[\frac{1}{Gz}-\frac{1}{B}\left(\cos\left(\frac{B}{Gz}\right)-1\right)\right] \tag{56}$$

where the ϕ_F is the average outlet temperature and it is defined as

$$\phi_F=-\frac{1}{V}\int_\kappa^1 u_b 2\pi R^2\eta\phi_b(\eta,0)d\eta \tag{57}$$

in flow pattern A, and

$$\phi_F = -\frac{1}{V}\int_0^{\kappa} u_a 2\pi R^2 \eta \phi_a(\eta,0)\mathrm{d}\eta \tag{58}$$

in flow pattern B, respectively. Therefore, the complete solutions of the temperature distribution in a double-pass concentric-tube heat exchanger were obtained by substituting the functions of θ_{0a}, θ_{0b}, θ_{1a}, θ_{1b}, θ_{2a}, θ_{2b}, θ_{3a} and θ_{3b} into the ϕ_a and ϕ_b, that is, Eqs. (14) and (15).

3. Heat-transfer efficiency improvement

The local Nusselt number of double-pass concentric-tube heat exchangers was defined as

$$Nu(\xi) = \frac{hD_e}{k} \tag{59}$$

where k is the heat conductivity coefficient of the wall, D_e is the equivalent diameter of the conduit, $D_e = 2R$, and h is the heat-transfer coefficient. The heat-transfer coefficient h was defined as

$$q''_w(z) = h(T_w(R,z) - T_i) \tag{60}$$

or, in the dimensionless form,

$$h = \frac{k}{R}\frac{q''_w(\xi)}{q''_0\phi_w(1,\xi)} = \frac{k}{R}\frac{1+\sin(B\xi)}{\phi_w(1,\xi)} \tag{61}$$

Substituting Eq. (61) into Eq. (59) yields

$$Nu(\xi) = \frac{2[1+\sin(B\xi)]}{\phi_w(1,\xi)} \tag{62}$$

Similarly, the local Nusselt number of single-pass tube heat exchangers was defined as

$$Nu_0(\xi) = \frac{2[1+\sin(B\xi)]}{\phi_{w0}(1,\xi)} \tag{63}$$

where the wall temperature distribution, $\phi_{w0}(1,\xi)$, of single-pass tube heat exchangers can be determined according to the reference [22].

Moreover, the average Nusselt numbers of single- and double-pass concentric-tube heat exchangers were determined by

$$\overline{Nu} = Gz\int_0^{1/Gz} Nu(\xi)\mathrm{d}\xi = Gz\int_0^{1/Gz}\frac{2[1+\sin(B\xi)]}{\phi_w(1,\xi)}\mathrm{d}\xi \tag{64}$$

and

$$\overline{Nu_0} = Gz\int_0^{1/Gz} Nu_0(\xi)\mathrm{d}\xi = Gz\int_0^{1/Gz}\frac{2[1+\sin(B\xi)]}{\phi_{w0}(1,\xi)}\mathrm{d}\xi \tag{65}$$

respectively. The heat-transfer efficiency improvement by employing a double-pass operation was defined as the percent increase in heat transfer based on that in a single-pass device with the same working dimensions and operating parameters

$$I_h = \frac{\overline{Nu} - \overline{Nu_0}}{\overline{Nu_0}}(\%) \tag{66}$$

4. Power consumption increment

The power consumption increases while an impermeable barrier is inserted into a single-pass device to conduct the double-pass operation. For simplicity to make a comparison, only the wall friction loss is considered in the calculation of the power consumption increment in double-pass devices. The friction losses caused by a joint, a diversion or a bending of a tube were neglected in this study. The wall friction loss can be estimated by

$$\ell w_f = 2f\bar{v}^2 L/D_e \tag{67}$$

in which $\bar{v}$ is the average velocity of fluid in the conduits. The friction factor f is determined by f=16/Re for the laminar flow in the circular conduits. The power consumption is determined by $P = V\rho\ell w_f$. Accordingly, the power consumption increment, I_p, of a double-pass device can be estimated based on the power consumption in a single-pass device as follows:

$$I_p = \frac{P-P_0}{P_0} = \frac{V\rho\left[\ell w_{f,a} + \ell w_{f,b}\right] - V\rho\ell w_{f,0}}{V\rho\ell w_{f,0}} = \frac{1}{\kappa^4} + \frac{1}{(1-\kappa^2)(1-\kappa)^2} - 1 \tag{68}$$

5. Results and discussion

The dimensionless temperature distributions of the laminar double-pass counterflow concentric-tube heat exchangers with sinusoidal wall fluxes were obtained by solving the energy balance equations with the aid of the linear superposition of Eqs. (14) and (15). The convergences of power series of Frobenius method in Eqs. (40) and (41) for flow patterns A and B are shown in Tables 1 and 2, respectively. The calculated results shown that the two finite series of n = 70 and 75 agree reasonably well for the power series because of the resulting average Nusselt numbers are the same for the cases of κ = 0.5 in flow patterns A and B, as indicated from Tables 1 and 2. Moreover, the convergence of Taylor series of $\ln\eta$ for N = 2 and 3 with κ = 0.5 in both flow patterns A and B are shown in Table 3 and the results indicate that the truncation after N = 2 of Taylor series for approximation of $\ln\eta$ is good enough. Therefore, the

Table 1
Convergence of power series in Eqs. (40) and (41) for n = 70 and 75 with κ = 0.5 (flow pattern A)

Gz	n	θ_{2a} (0.3)	θ_{3a} (0.3)	θ_{2b} (0.7)	θ_{3b} (0.7)	$\overline{Nu}$
1	70	−0.118	0.242	0.148	−1.524	0.09
	75	−0.118	0.242	0.148	−1.524	0.09
10	70	3.7×10^{-5}	9.1×10^{-6}	-5.0×10^{-4}	3.8×10^{-4}	2.34
	75	4.0×10^{-5}	-2.6×10^{-6}	-7.8×10^{-4}	7.9×10^{-4}	2.34
50	70	6.4×10^{-21}	1.5×10^{-21}	1.6×10^{-13}	-7.6×10^{-15}	6.62
	75	6.3×10^{-21}	-3.1×10^{-21}	2.6×10^{-14}	-1.1×10^{-15}	6.62
100	70	-2.2×10^{-24}	1.0×10^{-24}	1.7×10^{-13}	-8.1×10^{-15}	8.04
	75	-6.8×10^{-26}	3.3×10^{-26}	2.6×10^{-14}	-1.2×10^{-15}	8.04
200	70	-7.3×10^{-26}	1.4×10^{-25}	1.7×10^{-13}	-8.5×10^{-15}	8.99
	75	-7.8×10^{-27}	2.4×10^{-26}	2.7×10^{-14}	-1.3×10^{-15}	8.99

Table 2
Convergence of power series in Eqs. (40) and (41) for n = 70 and 75 with κ = 0.5 (flow pattern B)

Gz	n	θ_{2a} (0.3)	θ_{3a} (0.3)	θ_{2b} (0.7)	θ_{3b} (0.7)	$\overline{Nu}$
1	70	−0.118	0.242	0.148	−1.524	0.36
	75	−0.118	0.242	0.148	−1.524	0.36
10	70	3.7×10^{-5}	9.1×10^{-6}	-5.0×10^{-4}	3.8×10^{-4}	4.39
	75	4.0×10^{-5}	-2.6×10^{-6}	-7.8×10^{-4}	7.9×10^{-4}	4.39
50	70	6.4×10^{-21}	1.5×10^{-21}	1.6×10^{-13}	-7.6×10^{-15}	8.09
	75	6.3×10^{-21}	-3.1×10^{-21}	2.6×10^{-14}	-1.1×10^{-15}	8.09
100	70	-2.2×10^{-24}	1.0×10^{-24}	1.7×10^{-13}	-8.1×10^{-15}	9.00
	75	-6.8×10^{-26}	3.3×10^{-26}	2.6×10^{-14}	-1.2×10^{-15}	9.00
200	70	-7.3×10^{-26}	1.4×10^{-25}	1.7×10^{-13}	-8.5×10^{-15}	9.56
	75	-7.8×10^{-27}	2.4×10^{-26}	2.7×10^{-14}	-1.3×10^{-15}	9.56

terms of $n = 70$ and $N = 2$ were employed in the calculation procedure for the power series of Frobenius method and Taylor series, respectively, in this study.

5.1. Temperature distribution and Nusselt numbers in double-pass devices

For an engineer, to estimate the wall temperature of a heat exchanger for choosing the adequate heat exchanger materials is very important. Unfortunately, it is usually difficult to know the wall temperature of a heat exchanger with uniform or sinusoidal wall fluxes *in prior*. However, the dimensionless wall temperatures of the present design of double-pass heat exchangers with sinusoidal wall fluxes were obtained theoretically by solving the mathematical model analytically. The calculated results are illustrated in Figs. 2 and 3 for flow patterns A and B, respectively. Observing from Figs. 2 and 3, one can find that the wall temperature increases along the working fluid flowing direction due to the sinusoidal wall fluxes. Moreover, the working fluid has the longer residence time in conduit for lower Gz, i.e. lower volumetric flow rate or longer conduit length, resulting in the higher outlet temperature as confirmed by Eqs. (57) and (58). Hence, the profile of wall temperature varies more drastically and is higher in lower Graetz number than that in higher Graetz number. The influences of the impermeable-barrier location κ on the wall temperature are also shown in Figs. 2 and 3. The larger value of κ refers to the impermeable-barrier

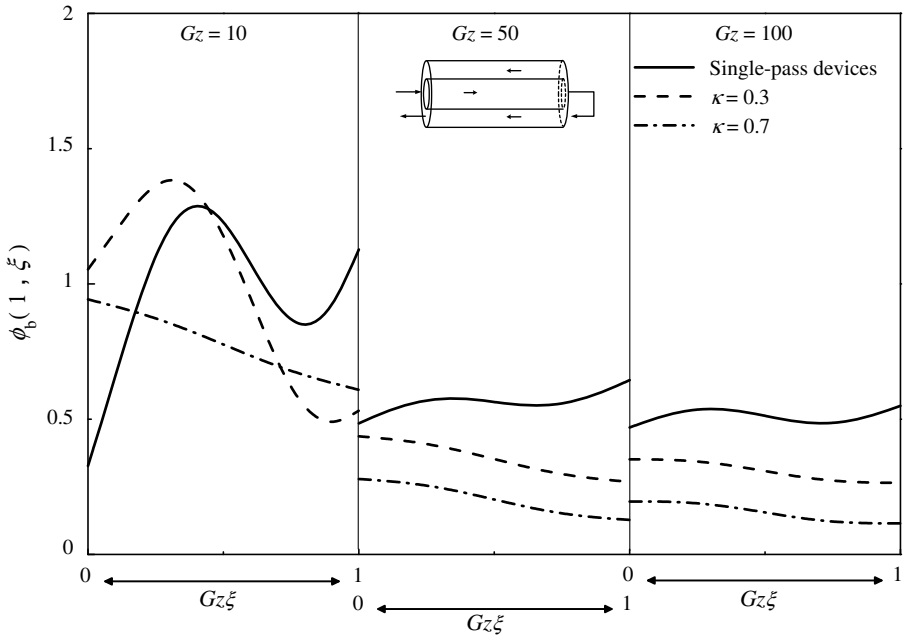

Fig. 2. Dimensionless wall temperature vs. $Gz\xi$ with κ as a parameter for $Gz = 10$, 50 and 100; flow pattern A.

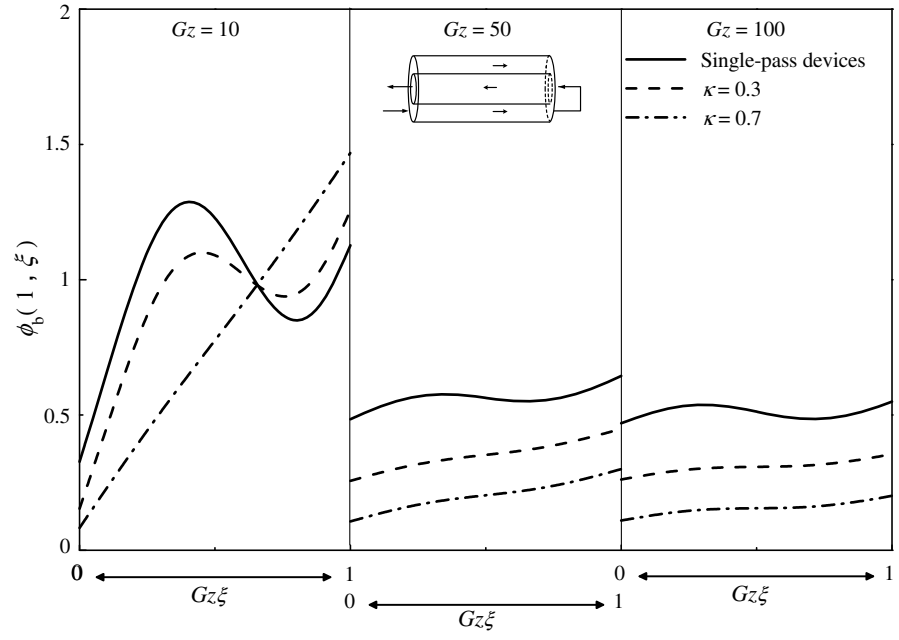

Fig. 3. Dimensionless wall temperature vs. $Gz\xi$ with κ as a parameter for $Gz = 10$, 50 and 100; flow pattern B.

Table 3
Convergence of Taylor series of $\ln\eta$ for $N = 2$ and 3 with $\kappa = 0.5$

Gz	N	Flow pattern A			Flow pattern B		
		θ_{2b} (0.7)	θ_{3b} (0.7)	$\overline{Nu}$	θ_{2b} (0.7)	θ_{3b} (0.7)	$\overline{Nu}$
1	2	0.148	−1.524	0.09	0.148	−1.524	0.36
	3	−0.012	−0.001	0.09	−0.012	−0.001	0.36
10	2	-5.0×10^{-4}	3.8×10^{-4}	2.34	-5.0×10^{-4}	3.8×10^{-4}	4.39
	3	-5.5×10^{-6}	3.7×10^{-5}	2.34	-5.5×10^{-6}	3.7×10^{-5}	4.39
50	2	1.6×10^{-13}	-7.6×10^{-15}	6.62	1.6×10^{-13}	-7.6×10^{-15}	8.09
	3	1.0×10^{-13}	-1.0×10^{-13}	6.62	1.0×10^{-13}	-1.0×10^{-13}	8.09
100	2	1.7×10^{-13}	-8.1×10^{-15}	8.04	1.7×10^{-13}	-8.1×10^{-15}	9.00
	3	1.5×10^{-13}	-1.2×10^{-13}	8.04	1.5×10^{-13}	-1.2×10^{-13}	9.00
200	2	1.7×10^{-13}	-8.5×10^{-15}	8.99	1.7×10^{-13}	-8.5×10^{-15}	9.56
	3	2.0×10^{-13}	-1.0×10^{-13}	8.99	2.0×10^{-13}	-1.0×10^{-13}	9.56

locate more near the outer tube, and hence, the average velocity in annulus tube $\bar{v}_b$ increases with κ. Moreover, due to the heat-transfer coefficient of working fluid is directly proportional to the fluid velocity, one can expect that the amount of heat removed from the wall increases with increasing κ. In other words, the wall temperature decreases with increasingκ, as confirmed by Figs. 2 and 3.

The Nusselt number represents the dimensionless quantity of heat-transfer coefficient and provides a measure of convection heat transfer occurring at the wall surface. The local Nusselt numbers of the double- and single-pass concentric-tube heat exchangers are determined by Eqs. (62) and (63), respectively. Figs. 4 and 5 show the local Nusselt number distributions of Flow patterns A and B, respectively, with κ as a parameter for $Gz = 10$, 50 and 100. Similar to the distribution of wall temperature, the distribution of local Nusselt numbers for a heat exchanger with sinusoidal wall fluxes is a sinusoidal curve as shown in Figs. 4 and 5. The local Nusselt numbers are inversely proportion to the wall temperature, as defined in Eqs. (62) and (63). Therefore, the local Nusselt numbers increase with the Graetz numbers and the impermeable-barrier location κ as illustrated in Figs. 4 and 5. The average Nusselt numbers of double- and single-pass are determined by Eqs. (64) and (65) and the results are shown in Figs. 6 and 7 for flow patterns A and B, respectively. The average Nusselt numbers increase with increasing Graetz numbers and the impermeable-barrier location κ, as shown in Figs. 4 and 5. Moreover, as referred to Eqs. (64) and (65), the $\overline{Nu}$ is inversely proportional to the average wall temperature, hence, the larger $\overline{Nu}$ also implies that the lower average wall temperature was obtained. The influence of constant B on the average Nusselt number in flow patterns A and B is shown in Table 4. The results indicate that the average Nusselt number is an increasing function of constant B in both flow patterns.

5.2. Heat-transfer efficiency improvement and power consumption increment

The heat-transfer efficiency improvement I_h by employing a double-pass operation is defined by Eq. (66). Some calculated results of I_h with κ as a parameter for flow pattern A and B are shown in Tables 5 and 6, respectively. The positive signs in Tables 5 and 6 refer that the heat-transfer efficiency of a double-pass device is higher than that of a single-pass device under the same operating conditions. Observing from Tables 5 and 6, one can find that the

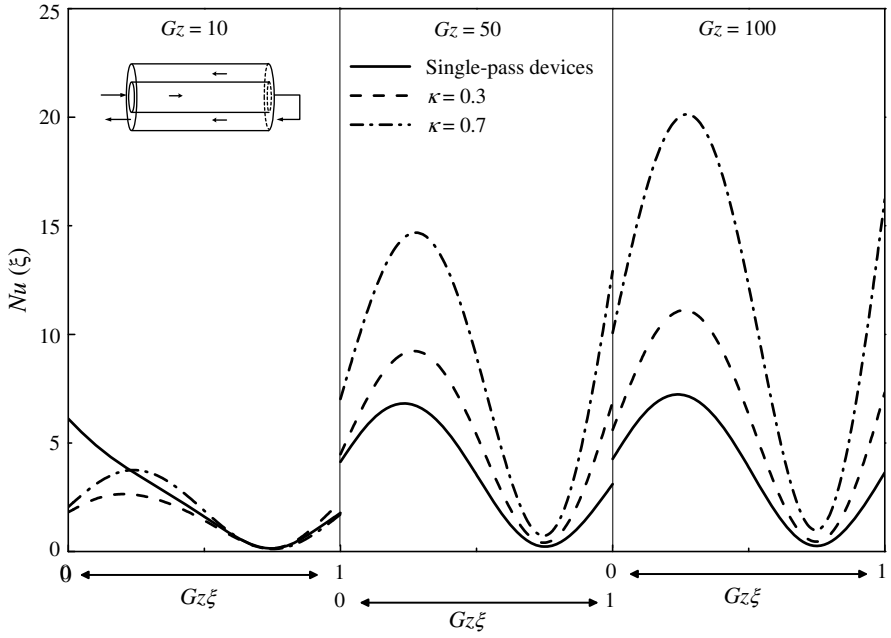

Fig. 4. The local Nusselt number vs. $Gz\xi$ with κ as a parameter for $Gz = 10$, 50 and 100; flow pattern A.

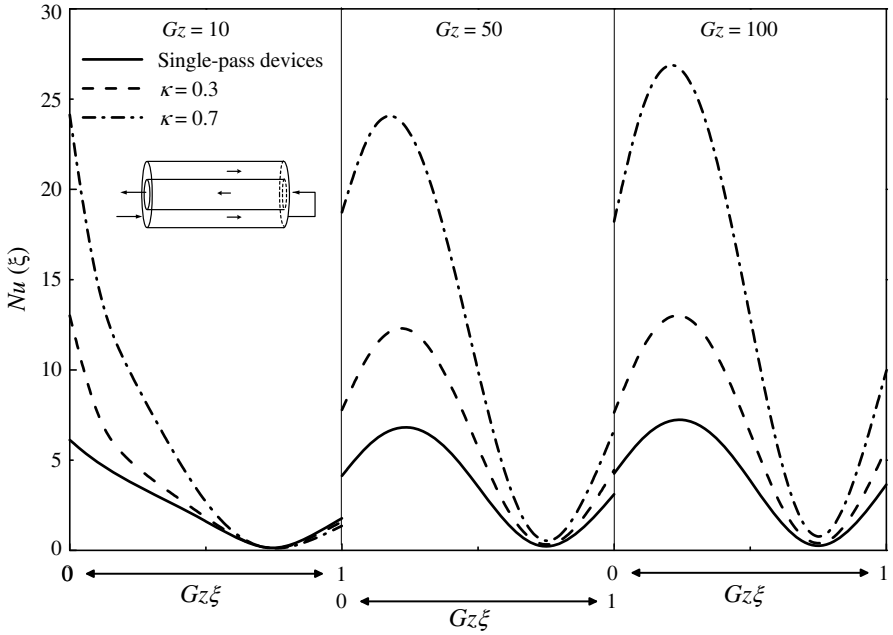

Fig. 5. The local Nusselt number vs. $Gz\xi$ with κ as a parameter for $Gz = 10$, 50 and 100; flow pattern B.

heat-transfer efficiency improvement increases with increasing Graetz numberGz and impermeable-barrier location κ. Moreover, Tables 4 and 5 also show the two results: (1) by employing flow pattern A, the positive heat-transfer efficiency improvement is obtained for $Gz > 10$ and $\kappa > 0.5$; (2) by employing flow pattern B, the positive heat-transfer efficiency improvement is obtained for $Gz > 10$.

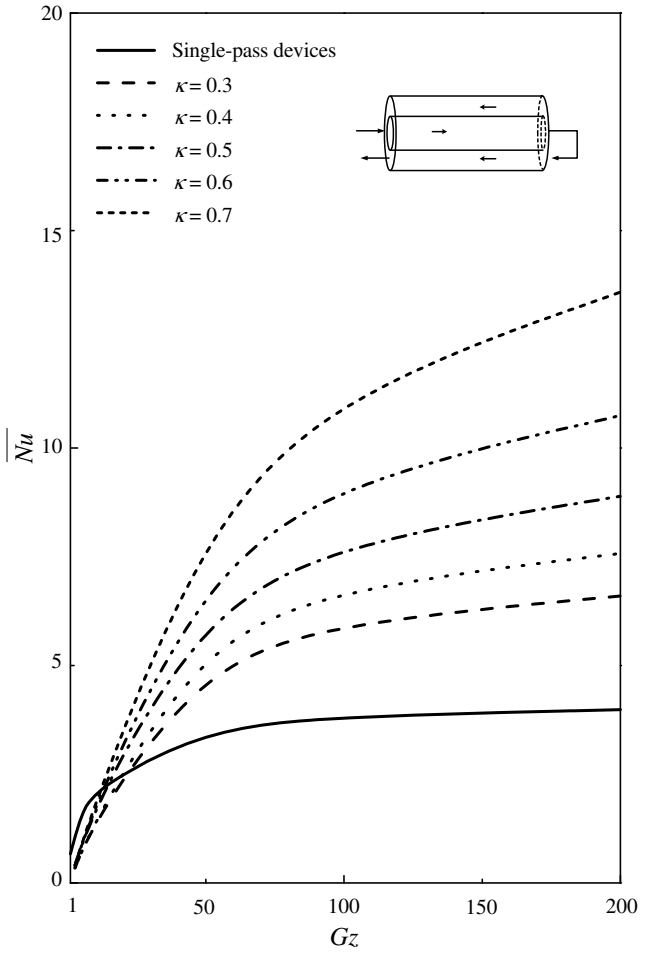

Fig. 6. The average Nusselt number vs. Gz with κ as a parameter; flow pattern A.

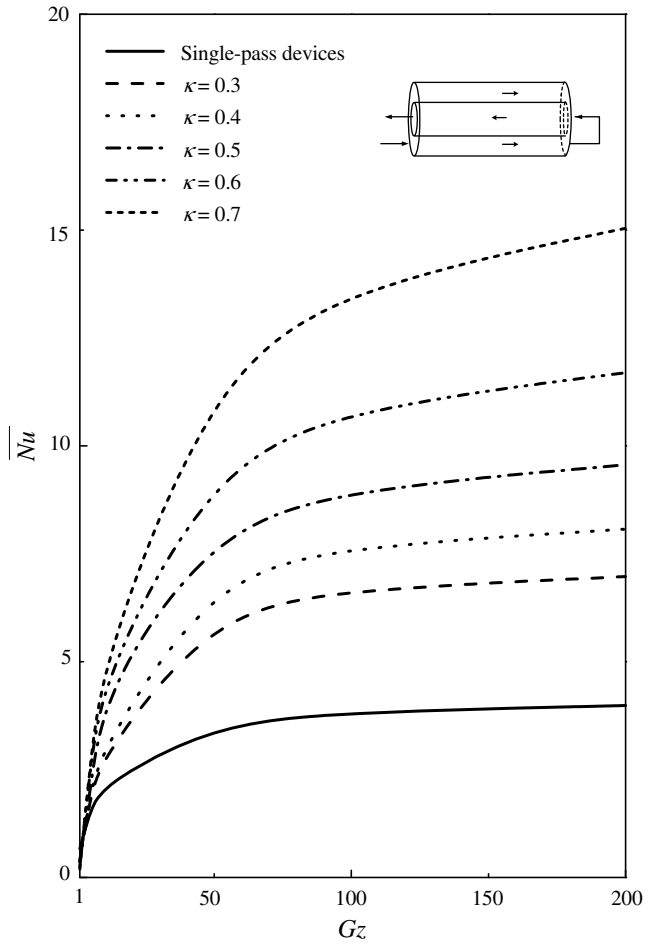

Fig. 7. The average Nusselt number vs. Gz with κ as a parameter; flow pattern B.

Table 4
Average Nusselt numbers with B as a parameter for $Gz = 100$

$\overline{Nu}$	$\kappa = 0.3$	$\kappa = 0.5$	$\kappa = 0.7$
Flow pattern A			
$B = 50$	6.85	8.67	12.42
$B = 100$	6.98	9.78	14.25
$B = 200$	7.78	10.13	14.56
Flow pattern B			
$B = 50$	5.45	11.07	15.09
$B = 100$	8.68	12.30	18.14
$B = 200$	9.45	13.31	20.50

Table 5
The heat-transfer efficiency improvement with κ as a parameter (flow pattern A)

I_h (%)	κ				
	0.3	0.4	0.5	0.6	0.7
$Gz = 1$	−82.64	−84.30	−86.70	−85.80	−84.49
10	−16.34	−16.24	7.82	9.61	11.73
100	59.48	81.24	109.61	148.43	205.04
200	67.01	92.06	125.58	173.02	245.59

Table 6
The heat-transfer efficiency improvement with κ as a parameter (flow pattern B)

I_h (%)	κ				
	0.3	0.4	0.5	0.6	0.7
$Gz = 1$	−39.85	−45.47	−46.28	−63.57	−71.01
10	32.80	42.26	102.63	118.43	139.19
100	74.07	100.11	134.78	183.56	257.52
200	74.93	102.49	139.78	193.42	277.31

For an economic sense, the power consumption increment cased by inserting an impermeable barrier into a single-pass device to conduct the double-pass operation is also discussed in this study. The power consumption increment I_p of a double-pass device is determined based on the power consumption in a single-pass device, as shown in Eq. (68). The power consumption increases with flow rate, tube diameter and fluid viscosity. Therefore, in an economic sense, the present double-pass device is suitable to the low viscosity fluid system under lower flow-rate operations. For example, under following working dimensions: $L = 1.2$ m, $R = 0.07$ m, $V = 1 \times 10^{-4}$ m^3/s, $\mu = 8.94 \times 10^{-4}$ kg/m s and $\rho = 997.08$ kg/m^3, the corresponding power consumption of a single-pass device is $P_0 = V\rho\ell w_{f,0} = 1.44 \times 10^{-6}$ J/s and Table 7 shows the calculating results of I_p. As indicated from Table 7, the I_p increases as κ moves away from 0.5. However, although the maximum power consumption increment is 10,000 for $\kappa = 0.1$, the corresponding power consumption $P = 1.44 \times 10^{-2}$ J/s is still small and it is reasonable to ignore the power consumption for all operation conditions. A comparison is made for the heat-transfer efficiency enhancement I_h and the power consumption increment I_p in the form of I_h/I_p. As shown in Fig. 8, for both flow patterns A and B, the values of I_h/I_p are positive as $Gz > 25$ and increase with increasing Graetz numberGz and impermeable-barrier location κ. Furthermore, comparing to both flow patterns by examining I_h/I_p, one can find that the flow pattern B always performs better than that in flow pattern A.

Table 7
The power consumption increment with κ as a parameter

I_p				
$\kappa = 0.1$	$\kappa = 0.3$	$\kappa = 0.5$	$\kappa = 0.7$	$\kappa = 0.9$
10,000	124	20	24	526

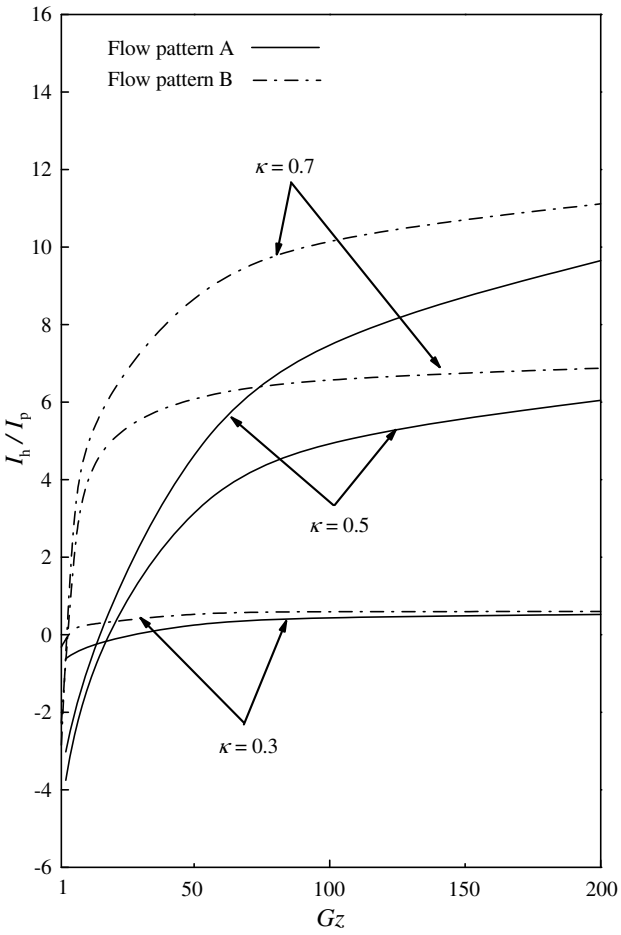

Fig. 8. The I_h/I_p vs. Gz with κ as a parameter; flow patterns A and B.

6. Conclusions

The theoretical mathematic model of the double-pass laminar counterflow concentric-tube heat exchangers with sinusoidal wall fluxes has been developed in this study. The heat-transfer phenomena of two flow patterns A and B are investigated theoretically in this study and it can be categorized to the conjugated Graetz problems. The analytical solutions are obtained by setting a general solution form for the laminar double-pass counterflow concentric-tube heat exchangers with sinusoidal wall fluxes [14,22] to separate the original boundary value problem into a partial differential equation, which can be solved by Frobenius method, and an ordinary differential equation. The influences of Graetz number Gz and impermeable-barrier location κ on the wall temperature distribution, local Nusselt number, average Nusselt number and heat-transfer efficiency improvement in a double-pass heat exchanger are also discussed in this study. The theoretical results indicate that the heat-transfer efficiency increases with increasing Gz and κ. In an economic sense, the best selection of operating conditions by considering both the heat-transfer efficiency enhancement and power consumption increment, i.e. I_h/I_p, are $Gz = 200$ and $\kappa = 0.7$, as shown in Fig. 8. Comparing to both flow patterns A and B, the flow pattern B achieves a good device performance than that in flow pattern A.

Acknowledgement

The authors thank the National Science Council of the Republic of China for its financial support.

Appendix A

By assuming the fully-developed laminar flow in each channel, steady-state and constant fluid physical properties, the momentum balance can be obtained by Navier–Stokes equation as follows:

$$-\frac{\mu}{r}\frac{\mathrm{d}}{\mathrm{d}r}\left(r\frac{\mathrm{d}u_{\mathrm{i}}}{\mathrm{d}r}\right)=-\frac{\mathrm{d}p_{\mathrm{i}}}{\mathrm{d}z}\quad(i=a,b) \tag{A1}$$

The boundary conditions in subchannel a of flow pattern A are

$$\frac{\mathrm{d}u_{\mathrm{a}}(0)}{\mathrm{d}r}=0\quad\text{and}\quad u_{\mathrm{a}}(\kappa R)=0 \tag{A2}$$

By integrating Eq. (A1) twice with respect to r and using the boundary condition Eq. (A2), one can get the velocity profile in subchannel a for flow pattern A

$$u_{\mathrm{a}}(r)=\frac{(\kappa R)^2}{4\mu}\left(-\frac{\partial p}{\partial z}\right)\left[1-\left(\frac{r}{\kappa R}\right)^2\right] \tag{A3}$$

Moreover, the corresponding average velocity is determined by

$$\bar{u}_{\mathrm{a}}=\frac{\int_0^{2\pi}\int_0^{\kappa_1 R}u_{\mathrm{a}}r\mathrm{d}r\mathrm{d}\theta}{\int_0^{2\pi}\int_0^{\kappa_1 R}r\mathrm{d}r\mathrm{d}\theta}=\frac{(\kappa R)^2}{8\mu}\left(-\frac{\partial P}{\partial z}\right)=\frac{V}{\pi(\kappa R)^2} \tag{A4}$$

Therefore, by substituting Eq. (A4) into (A3), one can get the velocity profile in subchannel a for flow pattern A, as shown in Eq. (3).

Furthermore, the boundary conditions in subchannel b of flow pattern A are

$$u_{\mathrm{b}}(\kappa R)=0\quad\text{and}\quad u_{\mathrm{b}}(R)=0 \tag{A5}$$

Following the same derivative procedure, the velocity profile in subchannel b for flow pattern A is thus obtained, as shown in Eq. (4). Similarly, the velocity profiles of flow pattern B in subchannels a and b can also be obtained by the same derivative procedure, as shown in Eqs. (5) and (6), respectively.

Appendix B

B.1. Flow pattern A

Substituting the velocity profiles, Eqs. (3) and (4), into Eqs. (34) and (35) gives the governing equations in flow pattern A as follows:

$$\eta\frac{\partial^2\psi_{\mathrm{a}}(\eta)}{\partial\eta^2}+\frac{\partial\psi_{\mathrm{a}}(\eta)}{\partial\eta}-\frac{B\eta}{2\kappa^2}\left[1-\left(\frac{\eta}{\kappa}\right)^2\right]\mathrm{i}\psi_{\mathrm{a}}(\eta)=0 \tag{B1}$$

$$\eta\frac{\partial^2\psi_{\mathrm{b}}(\eta)}{\partial\eta^2}+\frac{\partial\psi_{\mathrm{b}}(\eta)}{\partial\eta}+\frac{B\eta[1-\eta^2+W_2\ln\eta]}{2W_1(1-\kappa^2)}\mathrm{i}\psi_{\mathrm{b}}(\eta)=0 \tag{B2}$$

Firstly, taking Eq. (40) into Eq. (B1), one can get

$$\sum_{n=0}^{\infty}a_n(n+\lambda_{\mathrm{a}})^2\eta^{n+\lambda_{\mathrm{a}}-1}-\frac{Bi}{2\kappa^2}\left[\sum_{n=2}^{\infty}a_{n-2}\eta^{n+\lambda_{\mathrm{a}}-1}-\frac{1}{\kappa^2}\sum_{n=4}^{\infty}a_{n-4}\eta^{n+\lambda_{\mathrm{a}}-1}\right]=0 \tag{B3}$$

or

$$a_0\lambda_a^2\eta^{\lambda_{\mathrm{a}}-1}+a_1(1+\lambda_{\mathrm{a}})^2\eta^{\lambda_{\mathrm{a}}}+\left[a_2(2+\lambda_{\mathrm{a}})^2-\frac{Bi}{2\kappa^2}a_0\right]\eta^{\lambda_{\mathrm{a}}+1}+\left[a_n(3+\lambda_{\mathrm{a}})^2-\frac{Bi}{2\kappa^2}a_1\right]\eta^{\lambda_{\mathrm{a}}+2}+\sum_{n=4}^{\infty}\left[a_n(n+\lambda_{\mathrm{a}})^2-\frac{Bi}{2\kappa^2}a_{n-2}+\frac{Bi}{2\kappa^4}a_{n-4}\right]\eta^{n+\lambda_{\mathrm{a}}-1}=0 \tag{B4}$$

The indicial equation of Eq. (4) is

$$a_0\lambda_a^2=0 \tag{B5}$$

Because of $a_0\neq0$, the constant λ_{a} must equal to zero, i.e. $\lambda_{\mathrm{a}}=0$. Then, substituting $\lambda_{\mathrm{a}}=0$ into Eq. (B4) results

$$a_1+\left[4a_2-\frac{Bi}{2\kappa^2}a_0\right]\eta+\left[9a_3-\frac{Bi}{2\kappa^2}a_1\right]\eta^2+\sum_{n=4}^{\infty}\left[a_nn^2-\frac{Bi}{2\kappa^2}a_{n-2}+\frac{Bi}{2\kappa^4}a_{n-4}\right]\eta^{n-1}=0 \tag{B6}$$

By equating the coefficients of all η to zero, one can obtain two results. First, all the coefficients a_n with odd index must be zero

$$a_{2n+1}=0,\quad n\geqslant0 \tag{B7}$$

Second, the coefficients a_n with even index satisfy the recursive relation

$$a_{2n}=\frac{Bi}{8\kappa^2}\frac{1}{n^2}\left(a_{2n-2}-\frac{1}{\kappa^2}a_{2n-4}\right),\quad n\geqslant1 \tag{B8}$$

Moreover, the coefficient a_0 is the undetermined constant and it can be solved by the boundary conditions.

Then, taking Eq. (41) into Eq. (B2), one can get

$$\sum_{n=0}^{\infty}b_n(n+\lambda_{\mathrm{b}})^2\eta^{n+r-1}+\frac{Bi}{2W_1(1-\kappa^2)}\left[\sum_{n=0}^{\infty}b_n\eta^{n+\lambda_{\mathrm{b}}+1}-\sum_{n=0}^{\infty}b_n\eta^{n+\lambda_{\mathrm{b}}+3}+W_2\sum_{n=0}^{\infty}b_n(\eta^{n+\lambda_{\mathrm{b}}+1}\cdot\ln\eta)\right]=0 \tag{B9}$$

The term $\ln\eta$ in Eq. (B9) can be expressed in terms of Taylor series

$$\ln\eta=(\eta-1)-\frac{(\eta-1)^2}{2}+\frac{(\eta-1)^3}{3}+\cdots+\frac{(\eta-1)^N}{N} \tag{B10}$$

By taking the first two terms in Eq. (B10) and substituting $\ln\eta$ into Eq. (B9) result

$$\sum_{n=0}^{\infty}(n+\lambda_{\mathrm{b}})^2b_n\eta^{n+\lambda_{\mathrm{b}}-1}+\frac{Bi}{2W_1(1-\kappa^2)}\left[\sum_{n=2}^{\infty}\left(1-\frac{3W_2}{2}\right)b_{n-2}\eta^{n+\lambda_{\mathrm{b}}-1}+2W_2\sum_{n=3}^{\infty}b_{n-3}\eta^{n+\lambda_{\mathrm{b}}-1}-\sum_{n=4}^{\infty}\left(1+\frac{W_2}{2}\right)b_{n-4}\eta^{n+\lambda_{\mathrm{b}}-1}\right]=0 \tag{B11}$$

Following the same calculating procedure as presented before, one can find that the constant $\lambda_{\mathrm{b}}=0$ and the coefficients b_n are in the form

$$b_1=0,\quad b_n=\frac{-Bi}{2W_1(1-\kappa^2)}\frac{1}{n^2}\left[\left(1-\frac{3}{2}W_2\right)b_{n-2}+2W_2b_{n-3}-\left(1+\frac{1}{2}W_2\right)b_{n-4}\right],\quad n\geqslant2 \tag{B12}$$

B.2. Flow pattern B

Substituting the velocity profiles, Eqs. (5) and (6), into Eqs. (34) and (35) gives the governing equations in flow pattern B as follows:

$$\eta\frac{\partial^2\psi_{\mathrm{a}}(\eta)}{\partial\eta^2}+\frac{\partial\psi_{\mathrm{a}}(\eta)}{\partial\eta}+\frac{B\eta}{2\kappa^2}\left[1-\left(\frac{\eta}{\kappa}\right)^2\right]\mathrm{i}\psi_{\mathrm{a}}(\eta)=0 \tag{B13}$$

$$\eta\frac{\partial^2\psi_{\mathrm{b}}(\eta)}{\partial\eta^2}+\frac{\partial\psi_{\mathrm{b}}(\eta)}{\partial\eta}-\frac{B\eta[1-\eta^2+W_2\ln\eta]}{2W_1(1-\kappa^2)}\mathrm{i}\psi_{\mathrm{b}}(\eta)=0 \tag{B14}$$

Taking Eqs. (40) and (41) into Eqs. (B13) and (B14), respectively, and following the same calculating procedure, one can obtained the coefficients a_n

$$a_{2n} = \frac{-Bi}{8\kappa^2}\frac{1}{n^2}\left(a_{2n-2} - \frac{1}{\kappa^2}a_{2n-4}\right), \quad n \geqslant 1 \tag{B15}$$

and the coefficients b_n

$$b_1 = 0, \quad b_n = \frac{Bi}{2W_1(1-\kappa^2)}\frac{1}{n^2}\left[\left(1-\frac{3}{2}W_2\right)b_{n-2} + 2W_2 b_{n-3} - \left(1+\frac{1}{2}W_2\right)b_{n-4}\right], \quad n \geqslant 2 \tag{B16}$$

in flow pattern B.

References

[1] R.K. Shah, A.L. London, Laminar Flow Forced Convection in Ducts, Academic Press, New York, 1995. pp. 196–207.
[2] P.A. Ramachandran, Boundary integral solution method for the Graetz problem, Numer. Heat Transfer B 23 (1993) 257–268.
[3] A. Laouadi, N. Galanis, C.T. Nguyen, Laminar fully developed mixed convection in inclined tubes uniform heated on their outer surface, Numer. Heat Transfer A 26 (1994) 719–738.
[4] M.L. Michelsen, J. Villadsen, The Graetz problem with axial heat conduction, Int. J. Heat Mass Transfer 17 (1974) 1391–1402.
[5] S. Bilir, Numerical solution of Graetz problem with axial conduction, Numer. Heat Transfer A 21 (1992) 493–500.
[6] B. Weigand, An extract analytical solution for the extended turbulent Graetz problem with Dirichlet wall boundary conditions for pipe and channel flows, Int. J. Heat Mass Transfer 39 (1996) 1625–1637.
[7] M.A. Bernier, B.R. Baliga, Conjugate conduction and laminar mixed convection in vertical pipes for upward flow and uniform wall heat flux, Numer. Heat Transfer A 21 (1992) 313–332.
[8] M.R. Amin, J.A. Khan, Effects of multiple obstructions on conjugate forced convection heat transfer in tube, Numer. Heat Transfer A 26 (1996) 265–279.
[9] C.D. Ho, Y.C. Tsai, J.W. Tu, Improvement on device performance in multi-pass heat transfer through a parallel-plate channel with external recycle, Int. J. Heat Mass Transfer 50 (2007) 4805–4811.
[10] V.D. Zimparov, A.K. da Silva, A. Bejan, Thermodynamic optimization of tree-shaped flow geometries with constant channel wall temperature, Int. J. Heat Mass Transfer 49 (2006) 4839–4849.
[11] B. Weigand, D. Lauffer, The extended Graetz problem with piecewise constant wall temperature for pipe and channel flows, Int. J. Heat Mass Transfer 47 (2004) 5303–5312.
[12] A. Behzadmehr, N. Galanis, A. Laneville, Low Reynolds number mixed convection in vertical tubes with uniform wall heat flux, Int. J. Heat Mass Transfer 46 (2003) 4823–4833.
[13] O. Manca, S. Nardini, Experimental investigation on natural convection in horizontal channels with the upper wall at uniform heat flux, Int. J. Heat Mass Transfer 50 (2007) 1075–1086.
[14] C.D. Ho, S.C. Yeh, Improvement in device performance on laminar counterflow concentric circular heat exchangers with uniform wall fluxes, Int. J. Heat Mass Transfer 49 (2006) 2020–2032.
[15] D.A. Nield, Force convection in a parallel plate channel with asymmetric heating, Int. J. Heat Mass Transfer 49 (2004) 5609–5612.
[16] J. Maletic, B. Mitrovic, B.S. Baclic, Some peculiarities of the asymmetric Graetz problem, Int. J. Eng. Sci. 44 (2006) 436–455.
[17] J.N. Quaresma, R.M. Cotta, Exact solutions for thermally developing tube flow with variable wall heat flux, Int. Commun. Heat Mass Transfer 21 (5) (1994) 729–742.
[18] A. Barletta, E. Rossi di Schio, Effects of viscous dissipation on laminar forced convection with axially periodic wall heat flux, Heat Mass Transfer 35 (1999) 9–16.
[19] D.K. Choi, D.H. Choi, Dual solution for mixed convection in a horizontal tube under circumferentially non-uniform heating, Int. J. Heat Mass Transfer 35 (1992) 2053–2056.
[20] D.K. Choi, D.H. Choi, Developing mixed convection flow in a horizontal tube under circumferentially non-uniform heating, Int. J. Heat Mass Transfer 35 (1994) 1899–1913.
[21] C.J. Hsu, Heat transfer in a round tube with sinusoidal wall heat flux distribution, AIChE J. 11 (1965) 690–695.
[22] A. Barletta, Laminar forced convection with sinusoidal wall heat flux distribution: axially periodic regime, Heat Mass Transfer 31 (1995) 41–48.
[23] D.Y. Lee, S.J. Park, S.T. Ro, Heat transfer by oscillating flow in a circular pipe with a sinusoidal wall temperature distribution, Int. J. Heat Mass Transfer 38 (1995) 2529–2537.